Hindawi Publishing Corporation
Journal of Nanomaterials
Volume 2015, Article ID 980170, 7 pages
http://dx.doi.org/10.1155/2015/980170

Research Article

Synthesis and Ethanol Sensing Properties of Novel Hierarchical Sn_3O_4 Nanoflowers

Xingyang Li, Fengping Wang, Jianhai Tu, Hidayat Ullah Shah, Jianling Hu, Yan Li, Yanzhen Lu, and Mei Xu

Department of Physics, School of Mathematics and Physics, University of Science and Technology Beijing, Beijing 100083, China

Correspondence should be addressed to Fengping Wang; fpwang@ustb.edu.cn

Received 25 July 2015; Revised 8 November 2015; Accepted 17 November 2015

Academic Editor: Dojin Kim

Due to the metastable property and arduous preparation, to control the size and shape of intermediate Sn_3O_4 nanocrystals to tune functional properties still poses great challenge, and the physical and chemical properties are not fully investigated. Here, we report a simple one-pot template-free hydrothermal route to fabricate Sn_3O_4 flower-like hierarchical structures self-assembled by aligned high-density nanoslices. In order to explore the growth mechanism, a series of samples with various hydrothermal time were prepared and examined by FESEM and Raman. Results show that the hydrothermal time influences the phases and morphology of the final products. Particularly, a sensor based on these Sn_3O_4 was implemented to investigate the potential of Sn_3O_4 for the ethanol detection, revealing that this material reacts to ethanol in a linear way with high response yet at lower temperature (190°C) than that of the well-known SnO_2. Also, this intermediate tin oxide with rational control over dimension and morphology provides new opportunities for practical applications in gas sensing towards other reducing gases.

1. Introduction

SnO_x, with coordination structures including stoichiometric compounds SnO_2 and SnO, has drawn particular attention of researchers due to its excellent properties and great potential applications, such as lithium-ion battery, solar cell, photocatalyst, and gas sensor [1–5]. In addition, some nonstoichiometric compounds such as Sn_2O_3, Sn_3O_4, and Sn_5O_6, containing both the stannous (II) ion and the stannic (IV) ion, were predicted by theory [6]. In the same manner as other mixed-valence metal oxides such as Fe_3O_4 and Co_3O_4, these mixed-valence tin oxides might have a unique property and application in catalyst and lithium-ion battery [7, 8]. Among these multivalence tin oxides, Sn_3O_4 was first discovered by Lawson in 1967 [9]. In 2010, Sn_3O_4 was synthesized through the use of a carbothermal reduction method requiring a high temperature at 1,200°C and nitrogen atmosphere, which is difficult to implement [10]. For nearly two years, Sn_3O_4 has inspired new interests of researchers due to its promising properties in catalysis and gas sensor. In 2014, hierarchical Sn_3O_4 has been synthesized for the first time by a hydrothermal method and degraded all methyl orange within twenty minutes of being illuminated by visible light [11]. Manikandan et al. found that the H_2 evolution rate of Sn_3O_4 was greater than 5 μmolh^{-1}, which is competitive to the performance of reported visible-light-sensitive photocatalysts [12]. In 2015, researchers have demonstrated that the Sn_3O_4 nanobelt exhibits the ultrahigh sensitivity towards NO_2 at 200°C, over twice that of SnO_2 [13]. However, few reports have been focused on the study of Sn_3O_4, especially on the hydrothermal time's effects on the final product, due to its metastable property and arduous preparation.

Hydrothermal synthesis, due to its many advantages, such as short processing time, low growth temperature, easy control over experimental parameters, and convenience for large-scale synthesis, has been used to grow various advanced nanomaterials. In this study, we provided a simple, yet efficient, approach to prepare novel Sn_3O_4 nanoflowers consisting of nanoslices with a great crystallinity by facile hydrothermal synthesis mean. To propose the possible growth mechanism, we further investigated how the hydrothermal time influenced the final products, which

provided details on the formation of Sn_3O_4. In addition, gas sensor properties to ethanol and growth mechanism of Sn_3O_4 have also been investigated for the first time in detail.

2. Materials and Methods

2.1. Sample Preparation. In a typical preparation, 0.09 g SDS was melted in 20 mL NaOH (0.8 M) solution. Then, 20 mL $SnCl_2$ (0.2 M) solution was added into the above solution and stirred for 30 minutes. All the chemicals used were analytic pure without further purification. The acquired solution was transferred to a 50 mL Teflon-lined stainless autoclave, which was subsequently put into the electric oven, at the maintained temperature of 160°C, for 24 hours. After cooling down to the room temperature naturally, the yellow precipitate was collected and washed several times with distilled water and dried at 70°C for 12 hours.

2.2. Characterization. The morphology of the samples was analyzed by FESEM with an energy dispersive X-ray (EDX) spectroscopy (Field Emission Scanning Electron Microscopy, Hitachi S-3500) and TEM (Transmission Electron Microscopy, JEM-2010 200 KeV). The component, structure, crystallinity, and phase purity of the samples were examined by X-ray diffraction (X'Pert MPD), HRTEM (High Resolution Transmission Electron Microscopy), SAED (Selected Area Electron Diffraction), and Raman Spectroscopy (Horiba Jobin Yvon HR 800 Raman spectrometer, France). The excitation wavelength was 532 nm.

2.3. Fabrication of Gas Sensor. We fabricated the gas sensors by uniformly dispersing the mixture of powders and ethanol on the surface of a ceramic tube with a pair of previously printed gold electrodes that were connected by four platinum wires. Ni-Cr heating wire was inserted into the tube to manipulate the operating temperature by tuning the heating voltage. Figure 1 displays the schematic image of the as-prepared gas sensor. Next, the ceramic tube was fixed by wielding the ends of the six wires to the terminals of the pedestal and was aging inside the electric oven at 250°C, for 24 hours, before it was put into the chamber of the computer-controlled gas sensing machine (WS-30A gas sensing system, Weisheng Electronics Co., Ltd.). The environment relative humidity is 49% and ambient temperature is 19°C. The sensitivity of the sample is defined as R_a/R_g, where R_a and R_g stand for the resistance of sensor in the air and in the ethanol, respectively. The response and recovery times are defined as the time taken by the sensor reaching 90% of the equilibrium resistance.

3. Results and Discussion

Figures 2(a) and 2(b) depicted the morphology of the as-prepared sample examined by FESEM. The low-magnification FESEM image (Figure 2(a)) indicates a representative overview of the 3D uniform hierarchical flower-like architecture. Close examination by the high-magnification SEM, shown in Figure 2(b), reveals that

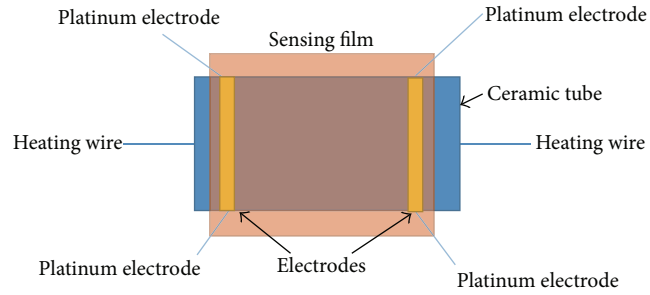

Figure 1: Schematic diagram of indirect-heating sensor.

the nanoflowers are self-assembled by well-defined thin nanoslices with sharp edges and smooth surfaces and the size of each nanoslice is about 5 μm.

The morphology was further verified by TEM (inset of Figures 2(b) and 2(c)). The inserted image in Figure 2 is a low-magnification TEM image, which further confirms that the nanoflowers are self-assembled by nanoslices being consistent with the result of FESEM. The thickness of a single slice that is approximately 8–15 nm was acquired by the high-magnification TEM image (Figure 2(c)). Further structural analysis of the Sn_3O_4 nanoslices was carried out by HRTEM (Figure 2(d)). From the HRTEM image, the measured fringe spacing of the nanoslice is 0.28 nm, which is very consistent with the d-value of 0.283 nm corresponding to (−210) crystal graphic planes of triclinic Sn_3O_4 (PDF 16-0737). Figure 2(d) is SAED patterns of a single sheet, clearly revealing that the nanoslices are monocrystal.

The structure of the as-acquired sample was measured by powder XRD as shown in Figure 3. All peak positions and intensities are consistent with the triclinic crystal structure Sn_3O_4 (PDF 16-0737), except for two weak peaks marked by (∗) and (○). These weak peaks reveal that the phase mainly consists of Sn_3O_4. The peak marked by (∗) is consistent with SnO (PDF 06-0395). The EDX spectrum (inset of Figure 3) confirms that the sample only consists of two elements, tin and oxygen (Cu is from substrate), which excludes the possibility that the peak (○) is caused by other elements. Because, theoretically, the structure of SnO_x reflects the arrangements of oxygen atoms and vacancies on the oxygen sublattice of the rutile SnO_2, the peak (○) is possible to be caused by the periodic oxygen defects near the surface or some new phase of SnO_x in the Sn_3O_4 structure, which agrees with the previous work [6, 14]. As a result, considering the uniform morphology of the as-prepared Sn_3O_4, we deduce that those weak peaks of XRD may be evidence of the heterojunctions of tin oxides.

Figure 4 was a Raman spectrum at room temperature, which provides structural information of the as-prepared sample. The two sharp peaks, centered at 143 and 172 cm^{-1}, respectively, are two characteristic phonon modes of Sn_3O_4 and other typical Raman modes of other tin oxides, mainly SnO (113 and 211 cm^{-1}) and SnO_2 (631 cm^{-1}), are absent, further revealing the high chemical and structural purity [10, 11, 15]. The peak at 241 cm^{-1} also belongs to the phase of Sn_3O_4 according to the previous work. A shoulder peak

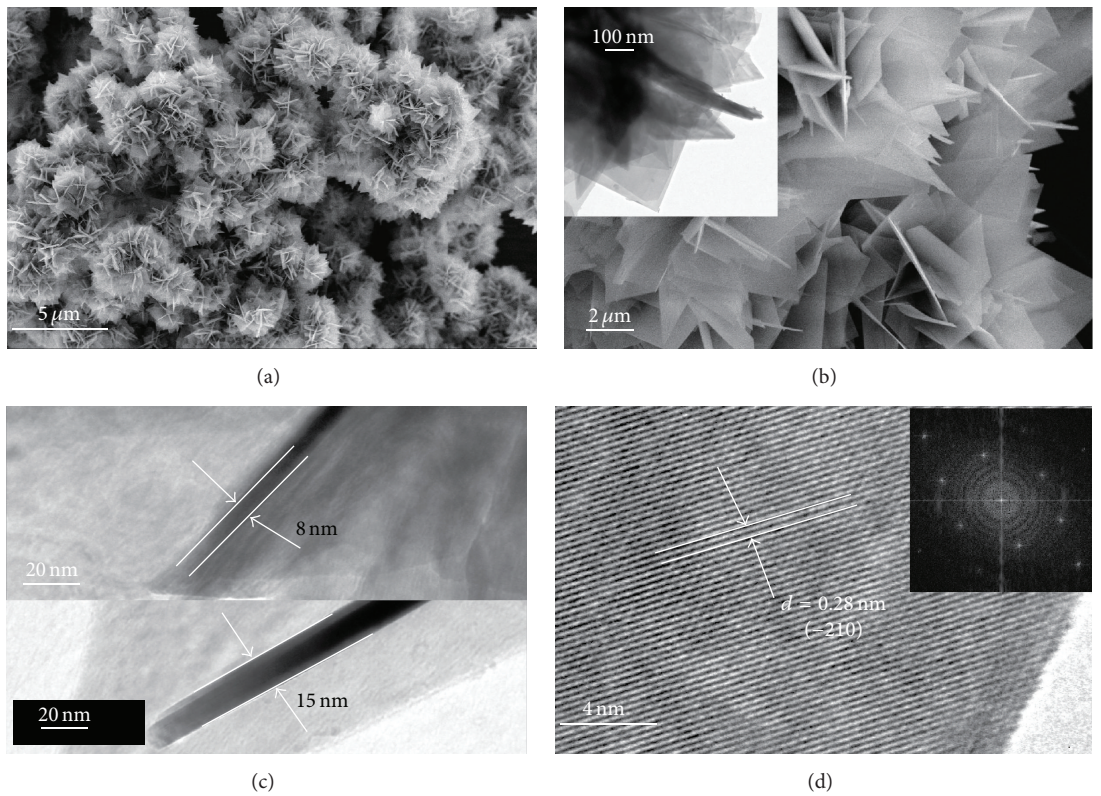

FIGURE 2: Structure information: (a, b) FESEM images, (inset of (b) and Figure (c)) TEM images of Sn_3O_4 nanopetal, (d) HRTEM image of a slice, and (inset of (d)) corresponding SAED patterns of the single nanoslice.

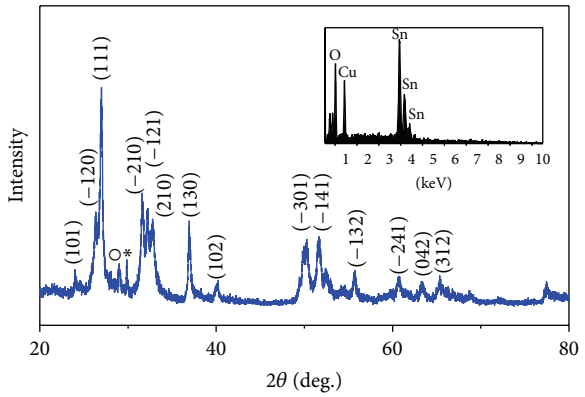

FIGURE 3: XRD patterns and the inset picture EDS of as-prepared sample.

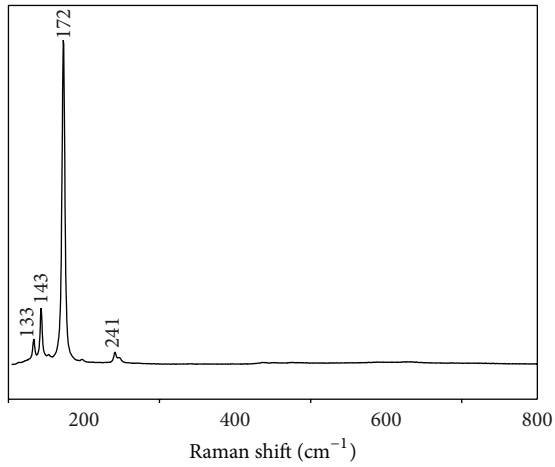

FIGURE 4: Raman spectrum of as-prepared sample.

at 133 cm^{-1} appears in most of the Raman spectra of Sn_3O_4, which may be another characteristic peak of Sn_3O_4 [10, 11, 16].

In order to investigate the growth mechanism of nanoflowers, a series of samples were acquired by altering hydrothermal time from 6 hours to 24 hours. All the samples were identified by the SEM and Raman spectra to determine chemical composition and morphologies, as shown in Figure 5. The SEM images show that, as the hydrothermal time is prolonged, the morphologies of the samples alter from the initially smooth, thick plates, to the porous, rough plates, and, ultimately, to the hierarchical nanoflowers. Also, the structure and chemical constitution of each sample from different hydrothermal stages vary. When the hydrothermal time is shorter than 6 h, the Raman spectrum shows a single peak at 210 cm^{-1}, revealing that the sample was exclusively composed of SnO. Extending the hydrothermal time to 12 h, two kinds of samples with different colors, one of which is yellow and the other is black, are acquired, respectively, being

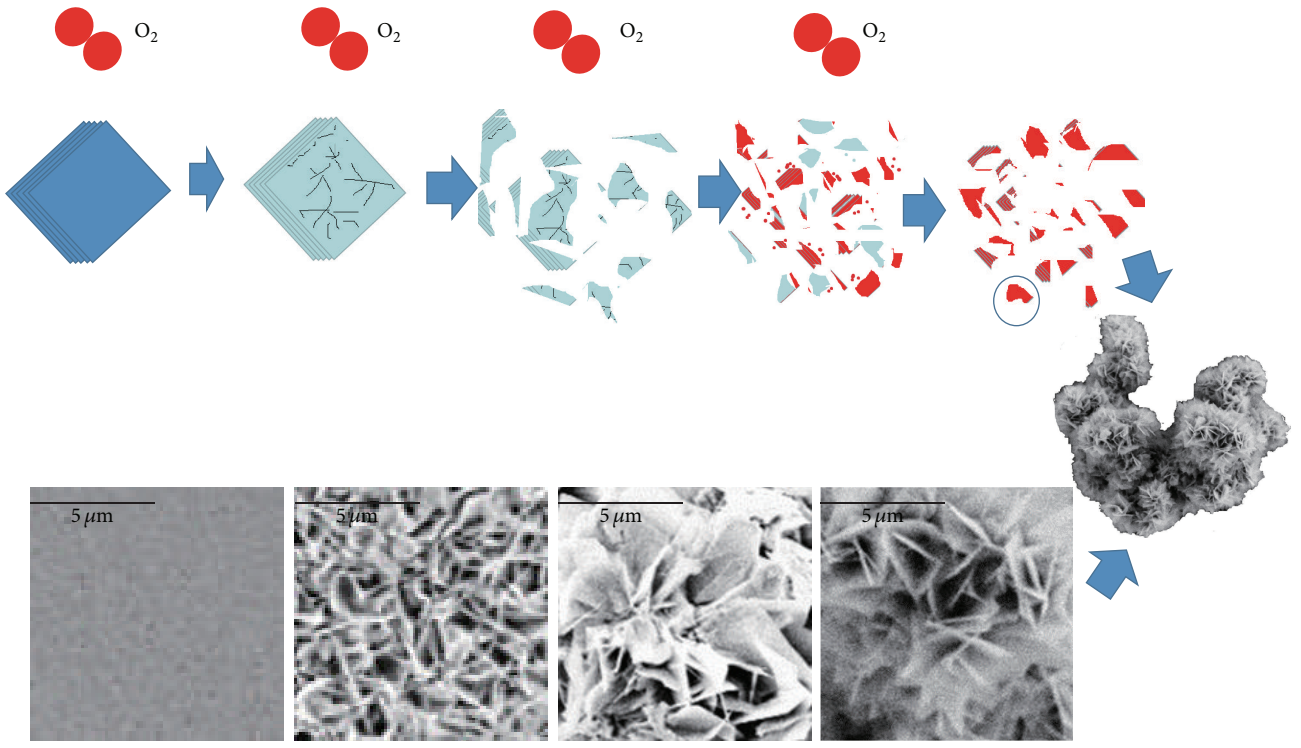

(a)

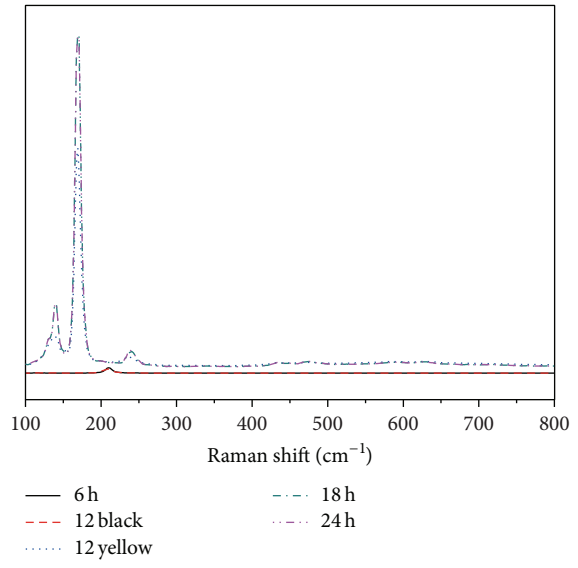

(b)

FIGURE 5: Growth mechanism of as-prepared sample; (a) morphology variation in response with operating time and pictures of possible growth mechanism (the red and the green represent the Sn_3O_4 and SnO, resp.) and (b) the Raman curve of samples at different hydrothermal times 6 h, 12 h, 18 h, and 24 h at room temperature.

testified to be SnO and Sn_3O_4 by the Raman peaks in 170 cm^{-1} and 210 cm^{-1}. Any sample with the hydrothermal time longer than 12 h sample is in the phase of Sn_3O_4. Based on those SEM images and structural information of the samples, a possible growth mechanism is proposed and displayed in Figure 5.

Consider the following:

(A) hydrolysis of SnCl2

$$4SnCl_2 + 2NaOH \longrightarrow Sn_4(OH)_2Cl_6 + 2NaCl \quad (1)$$

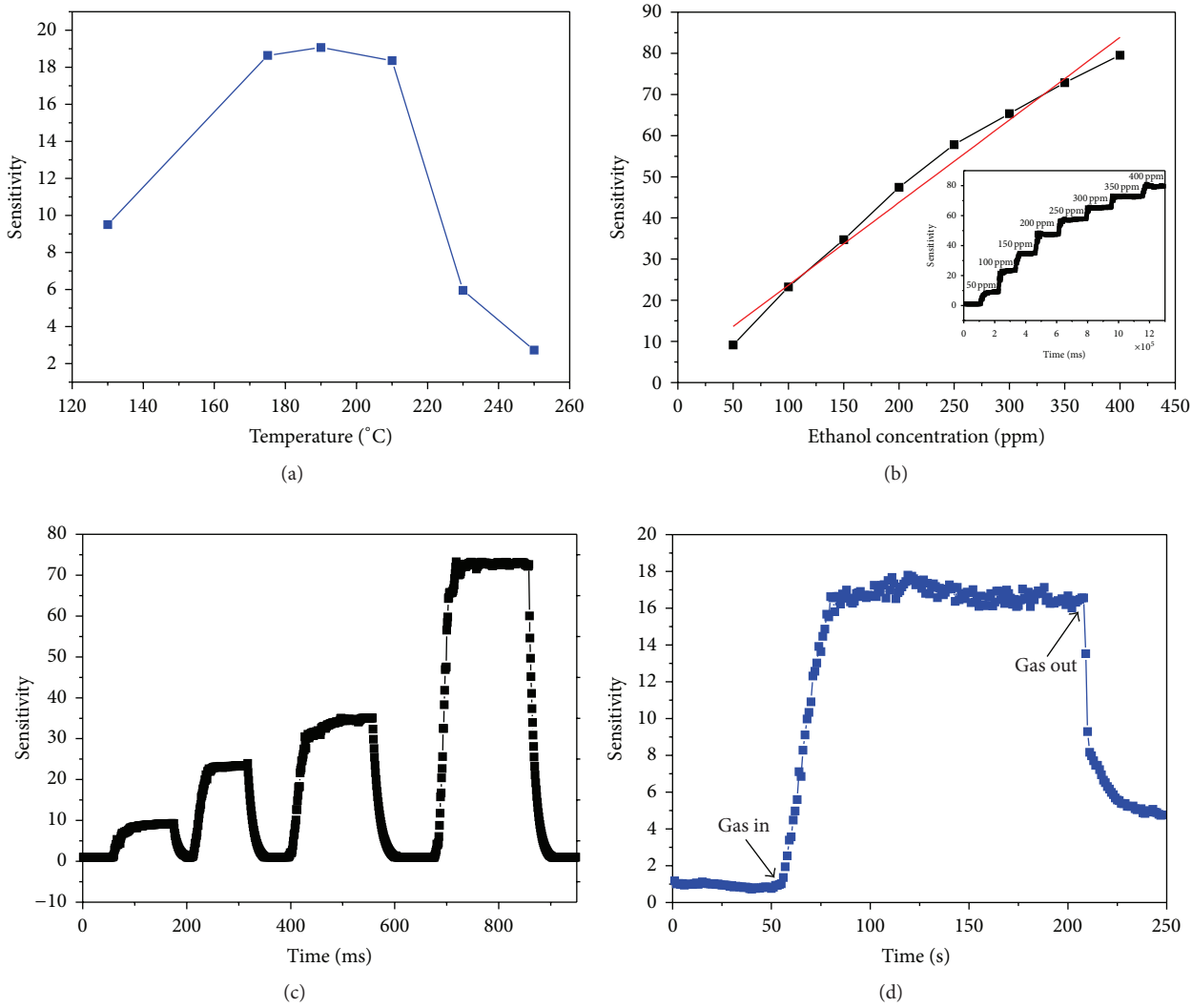

FIGURE 6: Gas sensitive response of as-prepared samples; (a) sensitivity variation in response with operating temperature; (b) the sensor response curve of gas sensor; (c) typical transient response curves of the sensors; and (d) dynamic sensing transient of the sensor to 100 ppm for ethanol.

(B) decomposition of Sn(OH)2Cl6

$$Sn_4(OH)_2Cl_6 + 6NaOH \longrightarrow 4SnO + 6NaCl + 4H_2O \quad (2)$$

(C) oxidization of tin monoxide

$$6SnO + 2O_2 \longrightarrow 2Sn_3O_4 \quad (3)$$

During the process of hydrothermal synthesis, the SnO comes into being first and, subsequently, the oxidation process begins. Obviously, the oxidation would increase the coordination number of tin atoms, altering the density of the samples. As a result, the microcracks gradually appeared on the surface or at the edge of the thick plates, rendering them coarse. Afterwards, the nonstop growing cracks, caused by the phase transition, result in the big plates breaking into the final flower-like small pieces.

In order to research the potential application of as-synthesized samples, a gas sensor was manufactured. It is well recognized that the operating temperature can greatly influence the gas sensor sensitivity. To determine the optimum temperature, the sensitivities of the gas sensor to 100 ppm ethanol at different temperatures ranging from 130 to 250°C were measured and shown in Figure 6(a). We can find that the sensitivity value reaches its maximum value of 18.75 at 190°C and then decreases with further increasing the temperature. Generally, the optimum temperature for tin dioxides is about 300°C [17, 18], while the as-prepared Sn_3O_4 exhibited sensitivity towards ethanol that is similar or even stronger than the reported SnO_2, but at a much lower optimum temperature 190°C [18, 19].

To further investigate the relationship between the gas concentration and the gas response, we present, in Figure 6(b), the gas response to ethanol with operating temperature of 190°C. As the gas concentration rises from 50 ppm to 400 ppm, the response of the sensor increases in nearly linear manner, without clues of the saturation, which is necessary

to monitor the concentration of the ethanol. The transient response characteristics of the flower-like architecture toward ethanol of different concentrations at 190°C were investigated and the results are displayed in Figure 6(c). The sensitivity increases dramatically as soon as the concentration of the gas increases, which exhibits high response and recovery property. Figure 6(d) shows the dynamic sensing transient of the sensor at the optimum temperature. By careful measurement, the response time of Sn_3O_4 and recovery time toward ethanol are approximately 20 and 60 seconds, respectively, which can meet the practical application.

Since the sensor sensitivity was defined as the ratio of the resistance in the air to the resistance in the gas, from Figure 6(d), we can deduce that the resistance of the materials drops, when the concentration of the ethanol increases, which agrees with the well-known gas sensitive behavior of n-type semiconductor materials [13]. Consequently, a probable mechanism of Sn_3O_4 is put forward, based on the representative mechanism of the n-type semiconductor. As we know, the fluctuation of the metal oxide-based sensors is governed absorption and depletion of the gas molecules on the surface of the material. During the process when the sensors are aging at the atmosphere, the surface of the material will absorb O_2 and the absorbed O_2 produces like O^-, O^{2-}, and O^{2-}, which trap electrons from conduction bands and generate an electron depletion on the surface, leading to high resistance [20, 21]. When the sensors are exposed to the reducing gas under appropriate operating temperature, for example, the ethanol in this paper, the reactions between the absorbed O_2 and the gas will take place on the surface of the materials, which decrease the concentration of the oxygen ions and thus release the restrained electron to the conduction band of the materials, giving rise to the decrease of the resistance. As observed in the SEM images, the unique 3D hierarchical shape presents a mesoporous structure. This mesoporous structure could provide abundant surface state and defects, as well as an enormous amount of mesopores with a highly active surface area. This large, specific surface area could more readily absorb gas molecules, which leads to the high gas sensor sensitivity and a faster response speed. In addition, the heterojunctions of tin oxides may play a role on its gas sensitive behavior.

4. Conclusions

To summarize, we successfully synthesize the novel hierarchical Sn_3O_4 via facile one-pot hydrothermal route and investigate the effects of the hydrothermal time on the phase of the final product, and its gas sensing properties. Experiment data shows that the hydrothermal time is the key factor to control the final chemical composition, especially when the metal element has many valences. In particular, the systematical study on the gas sensing indicates that, compared with traditional monovalence tin oxides, Sn_3O_4 reacts to the increase of the ethanol increase in a linear manner with a high response yet at a much lower temperature, which shows the great potential of the Sn_3O_4 for gas sensors towards other reducing gases.

Conflict of Interests

The authors have no conflict of interests regarding the issues discussed in this paper.

Acknowledgments

The authors appreciate the financial support of the National Natural Science Foundation of China (Grant no. 61373072), National Key Scientific Instruments and Equipment Development Special Fund (2011YQ14014506 and 2011YQ14014507), the Fundamental Research Funds for the Central Universities: FRF-BR-09-007A and FRF-BR-14-024A, and Beijing Higher Education Young Elite Teacher Project YETP0390.

References

[1] P. Gurunathan, P. M. Ette, and K. Ramesha, "Synthesis of hierarchically porous SnO_2 microspheres and performance evaluation as Li-Ion battery anode by using different binders," *ACS Applied Materials and Interfaces*, vol. 6, no. 19, pp. 16556–16564, 2014.

[2] H. K. Wang, K. P. Dou, W. Y. Teoh et al., "Engineering of facets, band structure, and gas-sensing properties of hierarchical Sn^{2+}-doped SnO_2 nanostructures," *Advanced Functional Materials*, vol. 23, no. 38, pp. 4847–4853, 2013.

[3] M. S. Wrighton, D. L. Morse, A. B. Ellis, D. S. Ginley, and H. B. Abrahamson, "Photoassisted electrolysis of water by ultraviolet irradiation of an antimony doped stannic oxide electrode," *Journal of the American Chemical Society*, vol. 98, no. 1, pp. 44–48, 1976.

[4] J. Long, W. Xue, X. Xie et al., "Sn^{2+} dopant induced visible-light activity of SnO_2 nanoparticles for H_2 production," *Catalysis Communications*, vol. 16, no. 1, pp. 215–219, 2011.

[5] C. Prasittichai and J. T. Hupp, "Surface modification of SnO_2 photoelectrodes in dye-sensitized solar cells: significant improvements in photovoltage via Al_2O_3 atomic layer deposition," *The Journal of Physical Chemistry Letters*, vol. 1, no. 10, pp. 1611–1615, 2010.

[6] A. Seko, A. Togo, F. Oba, and I. Tanaka, "Structure and stability of a homologous series of tin oxides," *Physical Review Letters*, vol. 100, no. 4, Article ID 045702, 2008.

[7] Y. Liang, Y. Li, H. Wang et al., "Co_3O_4 nanocrystals on graphene as a synergistic catalyst for oxygen reduction reaction," *Nature Materials*, vol. 10, no. 10, pp. 780–786, 2011.

[8] G. Zhou, D.-W. Wang, F. Li et al., "Graphene-wrapped Fe_3O_4 anode material with improved reversible capacity and cyclic stability for lithium ion batteries," *Chemistry of Materials*, vol. 22, no. 18, pp. 5306–5313, 2010.

[9] F. Lawson, "Tin oxide—Sn_3O_4," *Nature*, vol. 215, no. 5104, pp. 955–956, 1967.

[10] O. M. Berengue, R. A. Simon, A. J. Chiquito et al., "Semiconducting Sn_3O_4 nanobelts: growth and electronic structure," *Journal of Applied Physics*, vol. 107, no. 3, Article ID 033717, 2010.

[11] Y. He, D. Li, J. Chen et al., "Sn_3O_4: a novel heterovalent-tin photocatalyst with hierarchical 3D nanostructures under visible light," *RSC Advances*, vol. 4, no. 3, pp. 1266–1269, 2014.

[12] M. Manikandan, T. Tanabe, P. Li et al., "Photocatalytic water splitting under visible light by mixed-valence Sn_3O_4," *ACS Applied Materials & Interfaces*, vol. 6, no. 6, pp. 3790–3793, 2014.

[13] P. H. Suman, A. A. Felix, H. L. Tuller, J. A. Varela, and M. O. Orlandi, "Comparative gas sensor response of SnO_2, SnO and Sn_3O_4 nanobelts to NO_2 and potential interferents," *Sensors and Actuators, B: Chemical*, vol. 208, pp. 122–127, 2015.

[14] Z. R. Dai, Z. W. Pan, and Z. L. Wang, "Growth and structure evolution of novel tin oxide diskettes," *Journal of the American Chemical Society*, vol. 124, no. 29, pp. 8673–8680, 2002.

[15] F. Wang, X. Zhou, J. Zhou, T.-K. Sham, and Z. Ding, "Observation of single tin dioxide nanoribbons by confocal raman microspectroscopy," *The Journal of Physical Chemistry C*, vol. 111, no. 51, pp. 18839–18843, 2007.

[16] W. Xu, M. Li, X. B. Chen et al., "Synthesis of hierarchical Sn_3O_4 microflowers self-assembled by nanosheets," *Materials Letters*, vol. 120, pp. 140–142, 2014.

[17] X. Zhou, W. Fu, H. Yang, Y. Zhang, M. Li, and Y. Li, "Novel SnO_2 hierarchical nanostructures: synthesis and their gas sensing properties," *Materials Letters*, vol. 90, pp. 53–55, 2013.

[18] L. Xu, W. Chen, C. Wang, T. Gao, and Q. Zhou, "Facile hydrothermal synthesis and basic gas-sensing properties of two three-dimensional nanostructures of SnO_2," *Journal of Nanomaterials*, vol. 2014, Article ID 954734, 6 pages, 2014.

[19] B. Liu, L. Zhang, H. Zhao, Y. Chen, and H. Yang, "Synthesis and sensing properties of spherical flowerlike architectures assembled with SnO_2 submicron rods," *Sensors and Actuators, B: Chemical*, vol. 173, pp. 643–651, 2012.

[20] M. E. Franke, T. J. Koplin, and U. Simon, "Metal and metal oxide nanoparticles in chemiresistors: does the nanoscale matter?" *Small*, vol. 2, no. 1, pp. 36–50, 2006.

[21] S. M. Mohamed, "SnO_2 dendrites-nanowires for optoelectronic and gas sensing applications," *Journal of Alloys and Compounds*, vol. 510, pp. 119–124, 2012.